PHYSICAL REVIEW B **103**, 064421 (2021)

Positive exchange bias and inverted hysteresis loop in $Y_3Fe_5O_{12}/Gd_3Ga_5O_{12}$

Ravinder Kumar,[1] S. N. Sarangi,[2] D. Samal,[2,3] and Z. Hossain[1,*]
[1]*Department of Physics, Indian Institute of Technology, Kanpur 208016, India*
[2]*Institute of Physics, Sachivalaya Marg, Bhubaneswar 751005, India*
[3]*Homi Bhabha National Institute, Anushakti Nagar, Mumbai 400085, India*

(Received 31 August 2020; accepted 2 February 2021; published 15 February 2021)

We present evidence of an unprecedented room temperature positive exchange bias (EB) and hysteresis loop inversion in monolithic $Y_3Fe_5O_{12}$ films grown epitaxially on a (111)-oriented $Gd_3Ga_5O_{12}$ crystal. The growth-induced interfacial $Gd_3Fe_5O_{12}$ layer couples antiparallel to the $Y_3Fe_5O_{12}$ layer and leads to positive EB and in-turn loop inversion. An exchange shift as large as $H_{EB} \sim 30H_C$ is realized at 300 K. We observe a critical field value of $H_{CF} \sim 600$ Oe, above which the hysteresis loop inversion takes place. Our findings may have strong implication for spintronics device applications.

DOI: 10.1103/PhysRevB.103.064421

I. INTRODUCTION

$Y_3Fe_5O_{12}$ (YIG) with extremely low precessional damping ($\alpha \sim 7 \times 10^{-5}$) [1] is a potential candidate for the emerging field of spintronics and magnonics [2–11]. Coupling YIG with heavy metals gives birth to diverse spin-dependent phenomena such as spin pumping [3], the spin Seebeck effect [4], spin Hall magnetoresistance [7], the photo-spin-voltaic effect [8], etc. The magneto-optical activity and magnetocrystalline anisotropy can also be improved with bismuth or cerium doping [9–11]. Additionally, the magnetic properties change significantly with the tuning of thin film growth [1,6,9,12,13]. It has also been observed that the high growth and annealing temperature required for crystallization of YIG on top of lattice-matched $Gd_3Ga_5O_{12}$ (GGG) leads to the formation of a thin interfacial $Gd_3Fe_5O_{12}$ (GdIG) ferrimagnetic layer [14,15]. The interfaces in thin-film hybrids are known to trigger a wide range of intriguing phenomena such as interfacial superconductivity [16], two-dimensional electron gases [17], interfacial magnetism [18], and exchange bias (EB) [19–22]. A recent report on the YIG/GGG system with a growth-induced interfacial GdIG layer demonstrated an all-insulating equivalent of a synthetic antiferromagnet [15]. The YIG-GdIG heterostructure fabricated out of a monolithic YIG thin film has not been explored much, and a detailed magnetization study may engender fascinating interfacial magnetic functionalities.

EB is an interface-governed phenomenon and holds immense importance in the design and operation of many magnetic devices and sensors [23–26]. EB induces a hysteresis loop shift of a ferromagnetic (FM) layer in a specific direction depending on the interfacial exchange coupling with an adjacent antiferromagnetic (AFM) layer [27,28]. However, this effect has not been constrained to FM-AFM interfaces; coupled soft and hard FM layers could also give rise to this phenomenon [29–31]. A monolithic thin film with a growth-induced bilayer consisting of FM-AFM [19–21] or hard-soft FM [15,22] interfaces is of great interest for EB realization due to the ease of fabrication and sharp interfaces with high structural quality [15,19–22]. The interfaces may also lead to the occurrence of the very rare and interesting phenomenon of an inverted hysteresis loop (IHL), exhibiting negative coercivity H_C and remanence M_R values [20,21].

In this paper, we demonstrate room temperature positive EB and hysteresis loop inversion in a monolithic YIG thin film by virtue of AFM exchange coupling between YIG and the growth-induced interfacial GdIG layer. A detailed magnetization study reveals the critical field value mandatory for hysteresis loop inversion. Low-temperature magnetization measurement was employed to observe the variation in AFM coupling strength as the system crosses the GdIG layer compensation temperature. These findings in a YIG thin film enhance its application potential further for modern approaches to spintronics.

II. EXPERIMENTAL METHODS

YIG thin films were grown epitaxially on a (111)-oriented GGG substrate using a KrF Excimer laser (Lambda Physik COMPex Pro, $\lambda = 248$ nm) with a 20-ns pulse width. The substrates were *in situ* annealed at 800 °C in the presence of 4.0×10^{-2} mbar oxygen pressure for 120 min to get atomically flat surfaces. The laser was fired on a solid-state synthesized $Y_3Fe_5O_{12}$ target placed 50 mm away from the substrates at a repetition frequency of 10 Hz. The actual deposition was done after sufficient preablation of the YIG target to get a steady-state target surface. The YIG thin film was grown at room temperature and *ex situ* postannealed at 800 °C for 10 h in ambient air. X-ray diffraction (XRD) and X-ray reflectivity (XRR) were performed using a PANalytical X'Pert PRO four-circle diffractometer equipped with a Cu $K\alpha_1$ source ($\lambda = 1.54059$ Å). The hysteresis loops were traced using a superconducting quantum interface device (SQUID) based magnetometer (Quantum Design SQUID vibrating-sample

---

[*] zakir@iitk.ac.in

magnetometer). Utmost care was taken to avoid any contribution due to residual field. The magnet was demagnetized in an oscillation mode before each measurement. Also, a standard Pd sample was used as a reference material for calibration (residual field ~ -1 Oe).

III. RESULTS AND DISCUSSION

Figure 1 summarizes the structural analysis on a YIG thin film. The θ-2θ scan in Fig. 1(a) shows a (444) reflection of YIG and GGG. We observed a broad humplike feature beneath the YIG and GGG peaks. This broad feature appears due to the formation of a thin interfacial layer at the YIG-GGG interface. An expanded version [Fig. 1(b)] shows prominent trails of Laue oscillations, defining high structural quality. Further, high crystallinity is defined by very narrow full width at half maximum (FWHM) values (0.052° and 0.013° for YIG and GGG, respectively) obtained from the ω scan [Fig. 1(c)]. The formation of an interfacial layer due to the diffusion of elements at the interface is quite complex. Jakubisova *et al.* [14] suggested that the interface is more like GdIG, which couples antiferromagnetically with the rest of the YIG layer. Later, a report considered the interface consisting of a Gd and Gd-doped YIG layer which suppresses the net YIG magnetization [32]. A recent report by Gomez-Perez *et al.* [15] unambiguously confirmed the formation of a well-defined GdIG layer at the YIG-GGG interface. The study suggests that the magnetic moments of the interfacial hard GdIG layer couples strongly with the magnetic moments of the top soft YIG layer in an antiparallel manner. Figure 1(d) shows the XRR measurement on the YIG film. A perfect fit was achieved by considering two garnet layers with different elemental compositions, i.e., YIG and GdIG as the top bulk layer and thin interfacial layer, respectively. The XRR fitting gives 64.3-nm-thick YIG and 5.1-nm-thick GdIG layers. The θ-2θ XRD simulations around the (444) reflection match perfectly with the experimental pattern [Figs. 1(a) and 1(b), red: YIG, black: GdIG], and the thicknesses calculated for YIG and GdIG agree with the XRR fit.

Room temperature in-plane magnetization loops of the YIG/GdIG/GGG(111) sample are shown in Fig. 2, where the paramagnetic contribution from GGG was subtracted. Figure 2(a) shows series of $M(H)$ loops measured for different field ranges H_{FR} from ± 10 to ± 0.1 kOe in a sequence. The descending and ascending branches are shown by black and gray data points, respectively. For each $\pm H_{FR}$, the data were traced in the following sequence: $+H_{FR} \rightarrow 0 \rightarrow -H_{FR}$ (descending branch) $\rightarrow -H_{FR} \rightarrow 0 \rightarrow +H_{FR}$ (ascending branch). We observed a critical field H_{CF} above which the IHL is realized [21,33]. The left panel in Fig. 2(b) displays coercivity values for descending (H_C^{desc}) and ascending (H_C^{asc}) branches along with the net coercivity ($H_C = H_C^{\text{asc}} - H_C^{\text{desc}}$) as a function of H_{FR}. The H_C^{desc} and H_C^{asc} branches cross each other at certain field value, leading to a sign change of the net H_C. The H_C sign switches from positive to negative as H_{FR} increases and reveals a critical field, $H_{CF} \approx 600$ Oe [a zoomed-in version is shown in the right panel of Fig. 2(b)].

The observed IHL due to AFM exchange coupling between soft YIG and hard GdIG is explained as follows. The magnetization of the hard layer can be aligned only by applying an external field above H_{CF}. This indicates that the H_{CF} value extracted from Fig. 2(b) is the measure of anisotropy field associated with the hard magnetic layer. For the case $H_{FR} < H_{CF}$, the external field is sufficient to switch the magnetization of only the soft YIG layer, and hence, conventional loops are observed for H_{FR} below ± 0.5 kOe [Fig. 2(a)]. However, the AFM exchange coupling between soft and hard layers causes positive EB, leading to little loop shift. In positive EB, the $M(H)$ loop shifts in the direction of the initial scanning field; that is, for $\pm H_{FR}$ and $\mp H_{FR}$ (where $H_{FR} < H_{CF}$), the hysteresis loop shift occurs in the positive and negative directions, respectively. The progressive decrease of H_{FR} induces misalignment of the magnetic moments in the hard layer, due to which the loop shift at and below H_{CF} is not very prominent. Another magnetization measurement protocol is followed to observe the maximum positive EB shift, where the sample is first saturated at the $+10$ (-10) kOe field and then the hysteresis loop is measured for a field range of ± 0.1 (∓ 0.1 kOe); shown by red and black data in Fig. 2(c), respectively. The loop shift measured is quite large, $H_{EB} \approx \pm 30$ Oe, compared to the coercivity, $H_C \approx 1$ Oe. The loops shown in Fig. 2(c) for positive and negative saturation fields almost coincide with the descending and ascending branches of IHL measured for $H_{FR} = \pm 10$ kOe [shown in Fig. 2(a)], respectively. For the case $H_{FR} > H_{CF}$, the applied field is sufficient to switch the magnetization of both soft and hard layers in the same direction. At a field value higher than H_{CF}, magnetization of both the layers switches and gets aligned along the direction of the applied field, as shown in step M_1 of the schematic drawn in Fig. 2(d). The loop tracing begins from the initial field value shown by step M_1 in Fig. 2(d) by decreasing the applied field. As the field approaches H_{CF} and becomes lower than that, the magnetization of the soft layer starts to reverse gradually with the field direction, while the hard layer's magnetization remains aligned in the direction of the initial applied field. Since the AFM coupling between soft and hard layers is

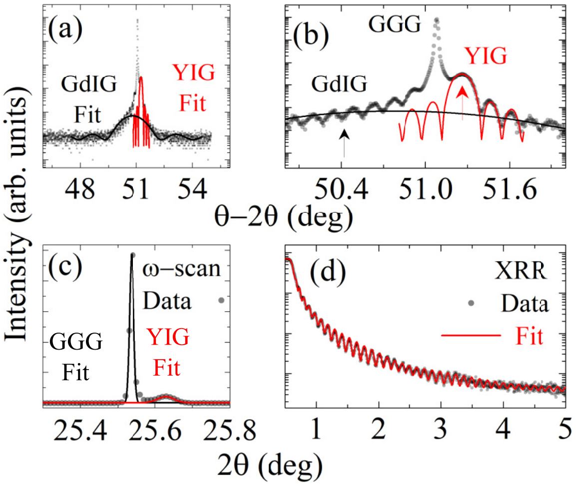

FIG. 1. (a) XRD θ-2θ scan on a YIG/GGG(111) sample with a growth-induced interfacial GdIG layer. (b) Laue oscillations [expanded version of (a)] and (c) an ω scan with narrow FWHM of YIG and GGG(444) reflections are the signature of high crystallinity. (d) XRR measurement on the YIG/GGG(111) sample with an interfacial GdIG layer.

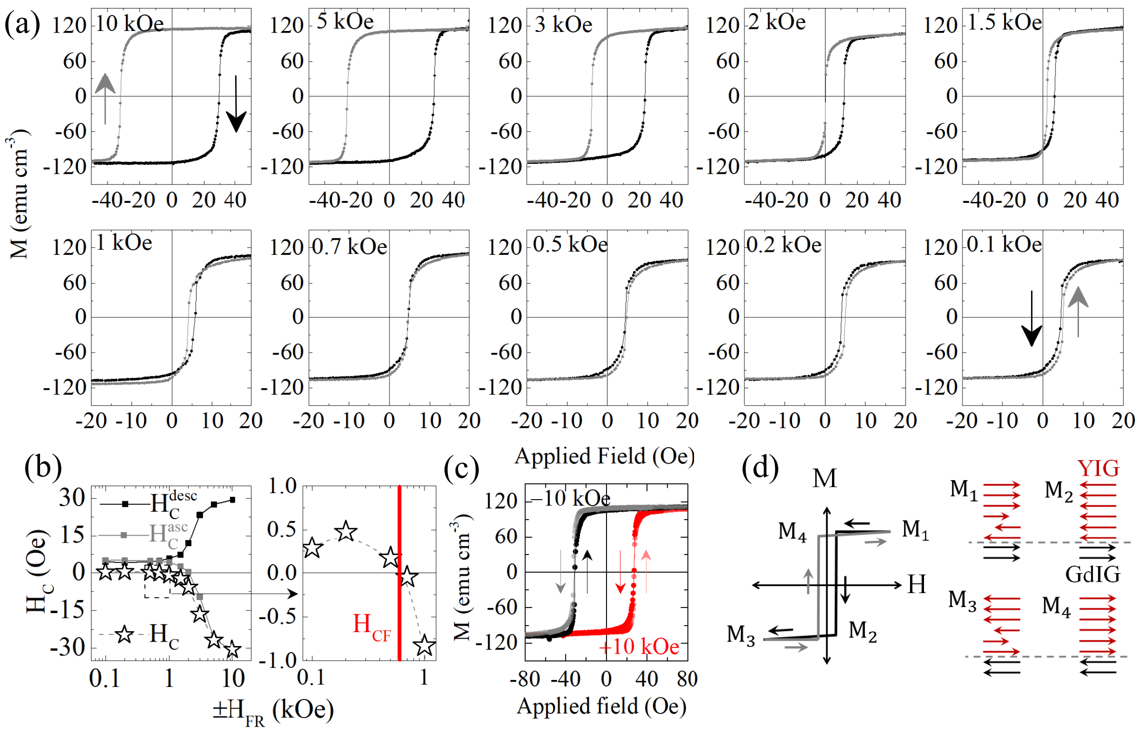

FIG. 2. Room temperature magnetization measurements on the YIG/GdIG/GGG(111) sample. (a) A series of $M(H)$ loops for different scanning field ranges from ±10 to ±0.1 kOe. The descending and ascending branches are represented by black and gray data points, respectively. (b) H_C^{desc}, H_C^{asc}, and H_C are plotted against H_{FR}: Coercivity changes from a positive to negative value with varying field (left panel). A zoomed-in version shows a critical field value for normal to inverted loop crossover (right panel). (c) Positive EB is realized by applying a saturation field of +10 (−10) kOe, and then the $M(H)$ loop is traced for a scanning field range of ±0.1 kOe, in red (∓0.1 kOe, in black). (d) Schematic representation of AFM exchange coupling between YIG and GdIG leading to IHL.

favorable, the soft-layer magnetization reversal is also favorable for energy minimization [21,33]. The AFM coupling leads to the soft-layer magnetization reversal at a lower energy; the descending branch falls in the positive quadrant with the moment arrangement shown by step M_2 in Fig. 2(d). Further application of high field in the negative direction to complete the tracing of the descending branch leads to the switching of the hard-layer magnetization. After the application of sufficient negative field, the magnetizations of both the soft and hard layers get aligned in the negative direction [step M_3 in Fig. 2(d)]. Similarly, starting from negative saturation, the ascending branch falls in the negative quadrant [step M_4 in Fig. 2(d)], completing the $M(H)$ loop with negative M_R and H_C.

To further substantiate the interfacial AFM coupling, we measured the temperature-dependent remnant magnetization $|M_R|$ of a YIG-GdIG heterostructure [shown in Fig. 3(a)]. The sample was subjected to a positive field (+10 kOe) to saturate the magnetization of both the layers in the same direction. The remnant magnetization was extracted from the $M(H)$ loops measured at different temperature in a field range of ±10 kOe. YIG consists of three sublattices, two magnetic due to Fe^{3+} and one nonmagnetic due to Y^{3+} [34]. The net magnetization in YIG appears due to AFM alignment of two iron sublattices, three tetrahedral and two octahedral Fe^{3+} ions per formula unit at d and a sites, respectively [34]. The three dodecahedral c sites per formula unit are occupied by Y^{3+} ions with no contribution to the net magnetization. However, in GdIG, the Y^{3+} is replaced by the Gd^{3+} ions, contributing to the net magnetization of GdIG. In GdIG the c-Gd^{3+} sublattice aligns ferromagnetically to a-Fe^{3+} and antiferromagnetically to d-Fe^{3+} [35]. The c-Gd^{3+} sublattices show strong temperature-dependent magnetization variation where the magnetization increases below room temperature [36,37]. The enhanced magnetization of the c-Gd^{3+} sublattice at a certain temperature T_{comp} along with the a-Fe^{3+} sublattice becomes equal to the magnetization of the d-Fe^{3+} sublattice and nullifies the net magnetization in GdIG, making it a compensated ferrimagnet [36,37]. T_{comp} may vary significantly depending on the film thickness, state of strain, and improper stoichiometry [36,37]. These factors may lead to a GdIG system which is not fully compensated. There will be a definite amount of magnetization at T_{comp}. Below T_{comp}, the net magnetization is driven by the FM coupling of c-Gd^{3+} and a-Fe^{3+} sublattices. Figure 3(b) consists of schematic representations of different magnetic and nonmagnetic sublattices in YIG and GdIG and the AFM coupling between YIG and GdIG for temperatures above (top panel) and below (bottom panel) T_{comp} of GdIG. For an applied field value below H_{CF}, the magnetization in both the layers is aligned antiparallelly. Above T_{comp}, the GdIG layer magnetization suppresses the total magnetization weakly. However, the suppression is strong

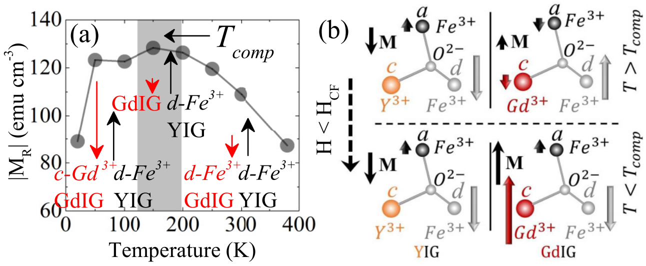

FIG. 3. (a) Remnant magnetization vs temperature showing the total magnetization suppression in AFM exchange coupled YIG and GdIG. The T_{comp} region for GdIG is shown by gray shading. (b) Different sublattices in YIG and GdIG and the AFM alignment between YIG and GdIG for applied field $H < H_{CF}$. Top: above T_{comp}; bottom: below T_{comp}.

below T_{comp} as the magnetization of the GdIG sublattice is enhanced significantly. The room temperature magnetization of the YIG-GdIG bilayer system is ~110 emu cm^{-3}, which is less than the value for a relatively thicker YIG film, ~130 emu cm^{-3} [12]. The AFM exchange coupling at the interface is responsible for the reduction of net magnetization in the YIG-GdIG bilayer system. The magnetization increases as the temperature decreases and attains a maximum value of ~128 emu cm^{-3} at ~150 K, the shaded region in Fig. 3(a). It is important to note that the magnetization near T_{comp} increases but not much and can be understood by considering the fact that the interfacial GdIG layer is extremely thin (~5 nm) and highly strained due to lattice distortion, which leads to a decrement in T_{comp} from ~288 K [36–38] to ~150 K. It is intuitive that the GdIG layer is not fully compensated and possesses magnetization near T_{comp}. The YIG and GdIG layers are still coupled antiferromagnetically. Further decrement in the temperature leads to rapid suppression of the total remnant magnetization as the GdIG layers magnetization increases drastically. This behavior can be understood only by considering an AFM coupling of the interfacial GdIG layer with the top YIG layer. The cartoons in Fig. 3(a) represent the change in AFM exchange coupling between YIG-GdIG as the temperature decreases. The net magnetization of GdIG layer decreases as the temperature decreases from 380 to 200 K and reaches the minimum within the compensation region. The magnetization of GdIG increases strongly after passing the T_{comp} region, resulting in the decrement of total magnetization due to AFM coupling between YIG and GdIG. A rough estimation of the hard-layer magnetization M_{hard} can be made by considering $M_{\text{hard}} = (M_1 + M_2)/2$, where M_1 and M_2 are defined in Fig. 2(d). M_{hard} of an ~5.1 nm GdIG layer calculated from the room temperature $M(H)$ loop, measured for $H_{FR} = \pm 10$ kOe, comes out to be ≈34 emu cm^{-3}, consistent with the values reported in the literature [36,38].

IV. CONCLUSIONS

In summary, an unconventional room temperature positive EB and hysteresis loop inversion were observed in an epitaxially grown monolithic YIG thin film. The growth process leads to the formation of an interfacial GdIG layer, providing an all-insulating ferrimagnetic garnet heterostructure developed from a monolithic YIG thin film. A series of magnetization measurements performed using different protocols revealed a critical field $H_{CF} \approx 600$ Oe above which the loop inversion takes place. The presence of positive EB, where the loop shift occurs in the direction of the applied saturation field, supports an AFM coupling between magnetically hard GdIG and soft YIG layers. This was further probed using a low-temperature remnant magnetization measurement, and the outcomes corroborate the fact that the bilayer system does possess AFM exchange coupling at the interface. Our work adds a striking feature to this technologically important insulating ferrimagnetic material.

ACKNOWLEDGMENT

Research support from IIT Kanpur and SERB, government of India (Grant No. CRG/2018/000220), is gratefully acknowledged. D.S. acknowledges the support from the Max Planck Partner Group. The authors thank B. Samantaray and P. Ghising for the valuable discussion.

---

[1] C. Hauser, T. Richter, N. Homonnay, C. Eisenschmidt, M. Qaid, H. Deniz, D. Hesse, M. Sawicki, S. G. Ebbinghaus, and G. Schmidt, Sci. Rep. **6**, 20827 (2016).

[2] Y. Kajiwara, K. Harii, S. Takahashi, J. Ohe, K. Uchida, M. Mizuguchi, H. Umezawa, H. Kawai, K. Ando, K. Takanashi, S. Maekawa, and E. Saitoh, Nature (London) **464**, 262 (2010).

[3] H. L. Wang, C. H. Du, Y. Pu, R. Adur, P. C. Hammel, and F. Y. Yang, Phys. Rev. Lett. **112**, 197201 (2014).

[4] K. Uchida, J. Xiao, H. Adachi, J. Ohe, S. Takahashi, J. Ieda, T. Ota, Y. Kajiwara, H. Umezawa, H. Kawai, G. E. W. Bauer, S. Maekawa, and E. Saitoh, Nat. Mater. **9**, 894 (2010).

[5] A. V. Chumak, V. I. Vasyuchka, A. A. Serga, and B. Hillebrands, Nat. Phy. **11**, 453 (2015).

[6] H. Wang, C. Du, P. C. Hammel, and F. Yang, Phys. Rev. B **89**, 134404 (2014).

[7] H. Nakayama, M. Althammer, Y.-T. Chen, K. Uchida, Y. Kajiwara, D. Kikuchi, T. Ohtani, S. Geprägs, M. Opel, S. Takahashi, R. Gross, G. E. W. Bauer, S. T. B. Goennenwein, and E. Saitoh, Phys. Rev. Lett. **110**, 206601 (2013).

[8] D. Ellsworth, L. Lu, J. Lan, H. Chang, P. Li, Z. Wang, J. Hu, B. Johnson, Y. Bian, J. Xiao, R. Wu, and M. Wu, Nat. Phys. **12**, 861 (2016).

[9] R. Kumar, B. Samantaray, and Z. Hossain, J. Phys.: Condens. Matter **31**, 435802 (2019).

[10] L. E. Helseth, R. W. Hansen, E. I. Il'yashenko, M. Baziljevich, and T. H. Johansen, Phys. Rev. B **64**, 174406 (2001).

[11] A. Kehlberger, K. Richter, M. C. Onbasli, G. Jakob, D. H. Kim, T. Goto, C. A. Ross, G. Götz, G. Reiss, T. Kuschel, and M. Kläui, Phys. Rev. Applied **4**, 014008 (2015).

[12] R. Kumar, Z. Hossain, and R. C. Budhani, J. Appl. Phys. **121**, 113901 (2017).
[13] B. Bhoi, B. Kim, Y. Kim, M.-K. Kim, J.-H. Lee, and S.-K. Kim, J. Appl. Phys. **123**, 203902 (2018).
[14] E. L. Jakubisova, S. Visnovsky, H. Chang, and M. Wu, Appl. Phys. Lett. **108**, 082403 (2016).
[15] J. M. Gomez-Perez, S. Vélez, L. McKenzie-Sell, M. Amado, J. Herrero-Martín, J. López-López, S. Blanco-Canosa, L. E. Hueso, A. Chuvilin, J. W. A. Robinson, and F. Casanova, Phys. Rev. Applied **10**, 044046 (2018).
[16] N. Reyren, S. Thiel, A. D. Caviglia, L. F. Kourkoutis, G. Hammerl, C. Richter, C. W. Schneider, T. Kopp, A.-S. Rüetschi, D. Jaccard, M. Gabay, D. A. Muller, J.-M. Triscone, and J. Mannhart, Science **317**, 1196 (2007).
[17] A. Ohtomo and H. Y. Hwang, Nature (London) **427**, 423 (2004).
[18] M. Keunecke, F. Lyzwa, D. Schwarzbach, V. Roddatis, N. Gauquelin, K. Müller-Caspary, J. Verbeeck, S. J. Callori, F. Klose, M. Jungbauer, and V. Moshnyaga, Adv. Funct. Mater. **30**, 1808270 (2020).
[19] Y. Fan, K. J. Smith, G. Lüpke, A. T. Hanbicki, R. Goswami, C. H. Li, H. B. Zhao, and B. T. Jonker, Nat. Nanotechnol. **8**, 438 (2013).
[20] M. Saghayezhian, S. Kouser, Z. Wang, H. Guo, R. Jin, J. Zhang, Y. Zhu, S. T. Pantelides, and E. W. Plummer, Proc. Natl. Acad. Sci. USA **116**, 10309 (2019).
[21] P. Ghising, B. Samantaray, and Z. Hossain, Phys. Rev. B **101**, 024408 (2020).
[22] E. Popova, N. Keller, F. Jomard, L. Thomas, M.-C. Brianso, F. Gendron, M. Guyot, and M. Tessier, Eur. Phys. J. B **31**, 69 (2003).
[23] J. Nogués and I. K. Schuller, J. Magn. Magn. Mater. **192**, 203 (1999).
[24] D. Lacour, H. Jaffrès, F. Nguyen Van Dau, F. Petroff, A. Vaurès, and J. Humbert, J. Appl. Phys. **91**, 4655 (2002).
[25] C. Tsang, R. E. Fontana, T. Lin, D. E. Heim, V. S. Speriosu, B. A. Gurney, and M. L. Williams, IEEE Trans Magn. **30**, 3801 (1994).
[26] S. M. Wu, S. A. Cybart, D. Yi, J. M. Parker, R. Ramesh, and R. C. Dynes, Phys. Rev. Lett. **110**, 067202 (2013).
[27] W. H. Meiklejohn and C. P. Bean, Phys. Rev. **102**, 1413 (1956).
[28] W. H. Meiklejohn and C. P. Bean, Phys. Rev. **105**, 904 (1957).
[29] C. Binek, S. Polisetty, X. He, and A. Berger, Phys. Rev. Lett. **96**, 067201 (2006).
[30] D. Navas, J. Torrejon, F. Béron, C. Redondo, F. Batallan, B. P. Toperverg, A. Devishvili, B. Sierra, F. Castaño, K. R. Pirota, and C. A. Ross, New J. Phys. **14**, 113001 (2012).
[31] B. Hebler, P. Reinhardt, G. L. Katona, O. Hellwig, and M. Albrecht, Phys. Rev. B **95**, 104410 (2017).
[32] A. Mitra, O. Cespedes, Q. Ramasse, M. Ali, S. Marmion, M. Ward, R. M. D. Brydson, C. J. Kinane, J. F. K. Cooper, S. Langridge, and B. J. Hickey, Sci. Rep. **7**, 11774 (2017).
[33] T. Maity, D. Kepaptsoglou, M. Schmidt, Q. Ramasse, and S. Roy, Phys. Rev. B **95**, 100401(R) (2017).
[34] L.-S. Xie, G.-X. Jin, L. He, G. E. W. Bauer, J. Barker, and K. Xia, Phys. Rev. B **95**, 014423 (2017).
[35] R. Nakamoto, B. Xu, C. Xu, H. Xu, and L. Bellaiche, Phys. Rev. B **95**, 024434 (2017).
[36] J. Cramer, E.-J. Guo, S. Geprägs, A. Kehlberger, Y. P. Ivanov, K. Ganzhorn, F. Della Coletta, M. Althammer, H. Huebl, R. Gross, J. Kosel, M. Kläui, and S. T. B. Goennenwein, Nano Lett. **17**, 3334 (2017).
[37] T. Yamagishi, J. Awaka, Y. Kawashima, M. Uemura, S. Ebisu, S. Chikazawa, and S. Nagata, Philos. Mag. **85**, 1819 (2005).
[38] S. Geprägs *et al.*, Nat. Commun. **7**, 10452 (2016).